3-1-2013

Thin-Shell Mixing In Radiative Wind-Shocks And The L-x Similar To L-bol Scaling Of O-Star X-Rays

S. P. Owocki

J. O. Sundqvist

David H. Cohen
Swarthmore College, dcohen1@swarthmore.edu

K. G. Gayley

Monthly Notices
of the
ROYAL ASTRONOMICAL SOCIETY

MNRAS **429,** 3379–3389 (2013) doi:10.1093/mnras/sts599

Thin-shell mixing in radiative wind-shocks and the $L_x \sim L_{bol}$ scaling of O-star X-rays

S. P. Owocki,[1]⋆ J. O. Sundqvist,[1] D. H. Cohen[2] and K. G. Gayley[3]

[1]*Bartol Research Institute, Department of Physics & Astronomy, University of Delaware, Newark, DE 19716, USA*
[2]*Department of Physics & Astronomy, Swarthmore College, Swarthmore, PA 19081, USA*
[3]*Department of Physics, University of Iowa, Iowa City, IA 52242, USA*

Accepted 2012 December 11. Received 2012 December 5; in original form 2012 July 31

ABSTRACT

X-ray satellites since *Einstein* have empirically established that the X-ray luminosity from single O-stars scales linearly with bolometric luminosity, $L_x \sim 10^{-7} L_{bol}$. But straightforward forms of the most favoured model, in which X-rays arise from instability-generated shocks embedded in the stellar wind, predict a steeper scaling, either with mass-loss rate $L_x \sim \dot{M} \sim L_{bol}^{1.7}$ if the shocks are radiative or with $L_x \sim \dot{M}^2 \sim L_{bol}^{3.4}$ if they are adiabatic. This paper presents a generalized formalism that bridges these radiative versus adiabatic limits in terms of the ratio of the shock cooling length to the local radius. Noting that the thin-shell instability of radiative shocks should lead to extensive mixing of hot and cool material, we propose that the associated softening and weakening of the X-ray emission can be parametrized as scaling with the cooling length ratio raised to a power m, the 'mixing exponent'. For physically reasonable values $m \approx 0.4$, this leads to an X-ray luminosity $L_x \sim \dot{M}^{0.6} \sim L_{bol}$ that matches the empirical scaling. To fit observed X-ray line profiles, we find that such radiative-shock-mixing models require the number of shocks to drop sharply above the initial shock onset radius. This in turn implies that the X-ray luminosity should saturate and even decrease for optically thick winds with very high mass-loss rates. In the opposite limit of adiabatic shocks in low-density winds (e.g. from B-stars), the X-ray luminosity should drop steeply with $\dot{M}^2$. Future numerical simulation studies will be needed to test the general thin-shell mixing ansatz for X-ray emission.

Key words: shock waves – stars: early-type – stars: mass-loss – stars: winds, outflows – X-rays: stars.

1 INTRODUCTION

Since the 1970s X-ray satellite missions like *Einstein*, *ROSAT*, and most recently *Chandra* and *XMM–Newton* have found hot, luminous, O-type stars to be sources of soft ($\lesssim$1 keV) X-rays, with a roughly[1] *linear* scaling between the X-ray luminosity and the stellar bolometric luminosity, $L_x \sim 10^{-7} L_{bol}$ (Chlebowski, Harnden & Sciortino 1989; Kudritzki et al. 1996; Berghoefer et al. 1997; Sana et al. 2006; Güdel & Nazé 2009; Nazé 2009; Nazé et al. 2011). In some systems with harder (a few keV) spectra and/or higher L_x, the observed X-rays have been associated with shock emission in colliding wind binary (CWB) systems (Stevens, Blondin & Pollock 1992; Gagné et al. 2012), or with magnetically confined wind shocks (Babel & Montmerle 1997; Wade 2012). But in putatively single, non-magnetic O-stars, the most favoured model is that the X-rays are emitted from *embedded wind shocks* that form from the strong, intrinsic instability (the 'line-deshadowing instability or LDI) associated with the driving of these winds by line scattering of the star's radiative flux (Owocki, Castor & Rybicki 1988; Feldmeier, Puls & Pauldrach 1997b; Dessart & Owocki 2003; Sundqvist & Owocki 2012).

This LDI can be simply viewed as causing some small ($\lesssim 10^{-3}$) fraction of the wind material to pass through an X-ray emitting shock, implying in the case that the full shock energy is suddenly radiated away such that the X-ray luminosity should scale with the wind mass-loss rate, $L_x \sim \dot{M}$. But within the standard Castor, Abbott & Klein (1975, hereafter CAK) model for such radiatively driven stellar winds, this mass-loss rate increases with luminosity[2] as $\dot{M} \sim L_{bol}^{1/\alpha} \sim L_{bol}^{1.7}$, where the latter scaling uses a typical CAK power index $\alpha \approx 0.6$ (Puls, Springmann & Lennon 2000). This then implies a *superlinear* scaling for X-ray to bolometric luminosity,

⋆ E-mail: owocki@bartol.udel.edu

[1] i.e. extending over 2 dex in L_{bol}, with a typical scatter of $\sim\pm 0.5$ dex

[2] For simplicity, this ignores a secondary scaling of luminosity with mass; see Section 3.4.

$L_x \sim L_{bol}^{1.7}$, which is too steep to match the observed, roughly linear law.

In fact, the above sudden-emission scaling effectively assumes that the shocks are *radiative*, with a cooling length that is much smaller than the local radius, $\ell \ll r$. In the opposite limit $\ell \gg r$, applicable to lower density winds for which shocks cool by *adiabatic* expansion, the shock emission scales with the X-ray *emission measure*, EM $\sim \int \rho^2 dV$, leading then to an even steeper scaling of X-ray versus bolometric luminosity, $L_x \sim \dot{M}^2 \sim L_{bol}^{3.4}$.

Both these scalings ignore the effect of bound-free absorption of X-rays by the cool, unshocked material that represents the bulk of the stellar wind. Owocki & Cohen (1999, hereafter OC99) showed that accounting for wind absorption can lead to an observed X-ray luminosity that scales linearly with L_{bol}, but this requires specifying ad hoc a fixed radial decline in the volume filling factor for X-ray emitting gas. We show below (Section 2.4) that this filling factor should actually be strongly affected by the level of radiative cooling. Moreover, while modern observations of spectrally resolved X-ray emission profiles by *Chandra* and *XMM–Newton* do indeed show the expected broadening from shocks embedded in the expanding stellar wind, the relatively weak blue–red asymmetry indicates that absorption effects are modest in even the densest OB-star winds (Cohen et al. 2010, 2011). Since many stars following the $L_x - L_{bol}$ empirical law have weaker winds that are largely optically thin to X-rays (Cohen, Cassinelli & Macfarlane 1997; Nazé et al. 2011), it now seems clear that absorption cannot explain this broad L_x scaling.

The analysis here examines instead the role of radiative cooling, and associated thin-shell instabilities (Vishniac 1994; Walder & Folini 1998; Schure et al. 2009; Parkin & Pittard 2010), in mixing shock-heated material with cooler gas, and thereby reducing and softening the overall X-ray emission. As summarized in Fig. 1, for a simple parametrization that this mixing reduction scales with a power (the 'mixing exponent' m) of the cooling length, ℓ^m, we find that the linear $L_x - L_{bol}$ law can be reproduced by assuming $m \approx 0.4$. The development below quantifies and extends a preliminary conference presentation of this thin-shell mixing ansatz (Owocki et al. 2012).

Specifically, to provide a quantitative basis for bridging the transition between radiative and adiabatic shock cooling, Section 2 first analyses in detail the X-ray emission from a simplified model of a single, standing shock in steady, spherically expanding outflow. Section 3 then generalizes the resulting simple bridging law to account for thin-shell mixing, and applies this in a simple exospheric model to derive general scalings for X-ray luminosity from a wind with multiple, instability-generated shocks assumed to have a power-law number distribution in wind radius. A further application to computation of X-ray line profiles (Section 4) provides constraints on the mixing and shock-number exponents needed to match observed X-ray emission lines. Following a brief presentation (Section 5) of full integral solutions for X-ray luminosity to complement the general scaling laws in Section 3, Section 6 concludes with a brief summary and outlook for future work.

2 STANDING-SHOCK MODEL

2.1 Energy balance

Most previous analyses of X-rays from massive stars (e.g. Wojdowski & Schulz 2005; Cohen et al. 2011) have been cast in terms of a density-squared emission measure from some fixed volume filling factor for X-ray emitting gas (see however Krolik & Raymond 1985; Hillier et al. 1993; Feldmeier et al. 1997a; Antokhin, Owocki & Brown 2004). So let us begin by showing

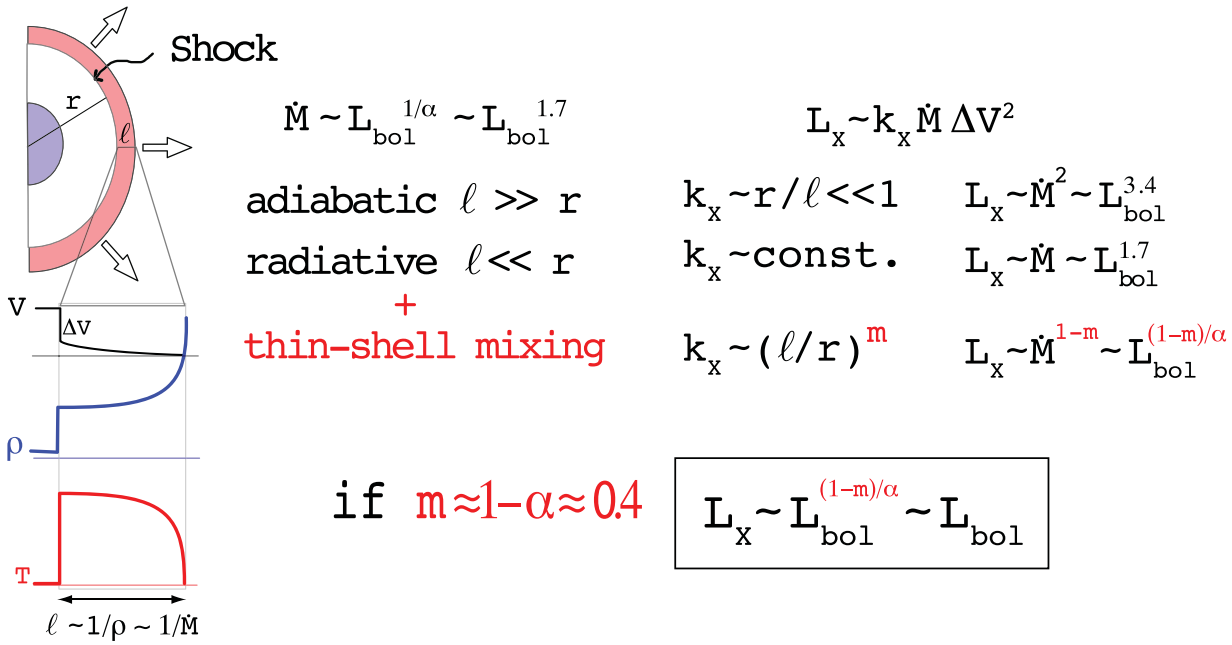

Figure 1. Summary sketch of the key concepts and results of the scaling analysis in this paper. The illustration of the cooling zone from a wind shock shows associated scalings for X-ray luminosity L_x with mass-loss rate $\dot{M}$ and bolometric luminosity L_{bol}, based on the conversion factor k_x of wind kinetic energy into X-rays, which for radiative shocks is a constant, but for adiabatic shocks is reduced by the ratio of the radius to cooling length, $r/\ell \ll 1$. (See equation 12 in the text.) In addition, thin-shell mixing of such radiative shocks is then posited to lead to a reduction of the X-ray emitting fraction that scales as a power law of the cooling length, $k_x \sim \ell^m$. For CAK wind index α, a mixing exponent $m = 1 - \alpha$ leads to the observationally inferred linear scaling of X-rays with bolometric luminosity, $L_x \sim L_{bol}$.

explicitly how that picture must be modified to account for the effects of radiative cooling, which can be important and even dominant for O-star wind shocks.[3] By focusing on the simple example of a steady, *standing* wind-shock, it is possible to carry out an analytic analysis that derives, more or less from first principles, a simple bridging law between the scalings for adiabatic versus radiative shocks.

Specifically, let us consider an idealized model in which a spherically symmetric, steady-state stellar wind with mass-loss rate $\dot{M}$ and constant, highly supersonic flow speed V_∞ undergoes a strong, standing shock at some fixed radius $r = r_s$. Relative to an unshocked wind with density $\rho_w = \dot{M}/4\pi V_\infty r^2$, the post-shock flow at $r > r_s$ has a density that is a factor $\rho/\rho_w = 4$ higher, with a post-shock speed that is a factor $v/V_\infty = 1/4$ lower. The reduction in flow kinetic energy results in a high, immediate post-shock temperature,

$$T_s = \frac{3}{16}\frac{\mu V_\infty^2}{k} = 14\,\mathrm{MK}\left(\frac{V_\infty}{1000\,\mathrm{km\,s^{-1}}}\right)^2 , \tag{1}$$

where k is Boltzmann's constant and the latter evaluation assumes a standard molecular weight $\mu = 0.62 m_p$, with m_p the proton mass.

But following this sudden shock increase, the combined effects of adiabatic expansion and radiative cooling cause the flow temperature T to decrease outward. For pressure $P = \rho kT/\mu$ and internal energy density $e = (3/2)P$, the steady-state energy balance for a general vector velocity $\boldsymbol{v}$ is

$$\nabla\cdot(e\boldsymbol{v}) = -P\nabla\cdot\boldsymbol{v} - \rho^2\Lambda_m(T)\,, \tag{2}$$

where $\Lambda_m \equiv \Lambda/(\mu_e\mu_p)$, with $\Lambda(T)$ the optically thin cooling function (e.g. Smith et al. 2001), and μ_e and μ_p, respectively, the mean mass per electron and per proton.

In general, we should also include a detailed momentum equation to account for possible acceleration of the post-shock flow, for example from the inward pull of stellar gravity, or the outward push of the gas pressure gradient. But the analysis here is greatly simplified if we make the reasonable assumption that these two countervailing accelerations roughly cancel, and so give a *constant speed* $v = V_\infty/4$ for all $r > r_s$. For this case of a steady, spherical, constant-speed post-shock outflow, the vector energy equation (2) reduces to a simple differential equation for the decline in temperature with radius r,

$$\frac{dT}{dr} = -\frac{4}{3}\frac{T}{r} - \frac{2\mu}{3kv}\rho\Lambda_m(T)\,, \tag{3}$$

wherein the first and second terms on the right-hand-side, respectively, represent the effects of adiabatic expansion and radiative cooling. This can alternatively be cast in terms of a temperature scalelength,

$$\frac{1}{H_T} \equiv -\frac{1}{T}\frac{dT}{dr} = \frac{4}{3r} + \frac{\kappa_c\rho}{3}\,, \tag{4}$$

where

$$\kappa_c(T) \equiv \frac{8\mu\Lambda_m(T)}{kTV_\infty} \tag{5}$$

is a mass cooling coefficient (with CGS units $\mathrm{cm^2\,g^{-1}}$), defined as the *inverse* of a characteristic cooling column mass. The corresponding cooling length is given by $\ell = 4/\kappa_c\rho = 1/\kappa_c\rho_w$, defined such that the radiative and adiabatic cooling terms are equal[4] when $\ell = r$.

2.2 X-ray luminosity

For any local post-shock temperature T, let $f_x(T)$ represent the fraction of radiation emitted in an X-ray bandpass of interest. Neglecting for now any wind absorption, the total X-ray luminosity from this single standing shock is then given by radial integration of the associated X-ray emission,

$$L_{xs} = 4\pi\int_{r_s}^{\infty}\rho^2\Lambda_m(T)\,f_x(T)\,r^2\,dr\,. \tag{6}$$

Using (4), this can be recast as an integral over temperature,

$$L_{xs} = 12\pi\int_0^{T_s} r^3\,\frac{\rho^2\Lambda_m(T)}{4+\kappa_c(T)\rho r}\,f_x(T)\,\frac{dT}{T} \tag{7a}$$

$$\approx 48\pi r_s^3\,\frac{\rho_{ws}^2\Lambda_m(T_s)}{1+\kappa_{cs}\rho_{ws}r_s}\,f_x(T_s)\,\frac{\delta T_s}{2T_s}\,, \tag{7b}$$

where the latter approximation[5] uses single-point trapezoidal integration, assuming that f_x declines from its post-shock value $f_x(T_s)$ to zero over a temperature range δT_s from the initial post-shock temperature $T_s = T(r_s)$. Here $\rho_{ws} = \dot{M}/(4\pi V_\infty r_s^2)$ is the wind density just *before* the shock, and

$$\kappa_{cs} \equiv \kappa_c(T_s) = \frac{128\Lambda_m(T_s)}{3V_\infty^3} \tag{8a}$$

$$= 2\sqrt{3}\Lambda_m(T_s)\left(\frac{kT_s}{\mu}\right)^{-3/2} \tag{8b}$$

$$\approx 1000\,\frac{\mathrm{cm^2}}{\mathrm{g}}\,T_7^{-2} \approx 750\,\frac{\mathrm{cm^2}}{\mathrm{g}}\,T_{\mathrm{kev}}^{-2}\,, \tag{8c}$$

with $T_7 \equiv T_s/10^7\,K$ and $T_{\mathrm{kev}} \equiv kT_s/\mathrm{keV}$. The numerical evaluation in (8c) assumes an approximate fit to the cooling function, $\Lambda(T_s) \approx 4.4\times10^{-23}/\sqrt{T_7}\ \mathrm{erg\,cm^3\,s^{-1}}$, over the relevant range of shock temperatures, $10^{6.5}\,K < T_s < 10^{7.5}\,\mathrm{K}$ (Schure et al. 2009). Recall that the shock cooling length is set by $\ell_s = 1/\kappa_{cs}\rho_{ws}$.

For context, the mass absorption coefficient for bound-free absorption of X-rays when smoothed over bound-free edges, also roughly follows an inverse-square scaling with energy. Over the relevant energy range 0.5–2 keV, we can use the the opacity curves of, e.g. Cohen et al. (2010), Leutenegger et al. (2010) or Hervé et al. (2012) to write an approximate scaling form,

$$\kappa_{bf} \approx 30\,\frac{\mathrm{cm^2}}{\mathrm{g}}\,E_{\mathrm{kev}}^{-2}\,, \tag{9}$$

where E_{kev} is now the X-ray *photon energy* in keV.

By casting the cooling strength in an opacity form normally used to describe absorption, we are thus able to make direct comparisons

[3] This was actually noted explicitly by Zhekov & Palla (2007), but their results were nonetheless still cast in terms of a density-squared emission measure that is not appropriate for radiative shocks.

[4] The ratio ℓ/r differs only by an order-unity factor from the ratio of cooling to escape time, $\chi \equiv t_{cool}/t_{esc}$, defined by Stevens et al. (1992) to characterize the transition from radiative to adiabatic shocks in colliding stellar winds.

[5] Aside from $f_x(T)$, the combination of other factors in the integrand for (7a) becomes constant in T in the radiative limit $\kappa_c\rho r \gg 1$, and scales as $T^{-3/4}$ in the opposite, adiabatic limit. For $f_x(T)$ that declines roughly linearly with temperature, the approximate trapezoidal integration (7b) thus becomes nearly exact in the radiative limit, while mildly underestimating the actual value in the adiabatic limit, for example by about 15 per cent for $\delta T_s = T_s/2$.

between cooling and absorption, and so characterize their respective domains of importance. This is further facilitated by the quite fortunate coincidence that both have similar inverse-square scalings with their associated energy.

Since these respective energies are usually roughly comparable, $E_{\rm kev} \approx T_{\rm kev}$, the fact that the numerical factor for $\kappa_{\rm cs}$ is about 25 times greater than for $\kappa_{\rm bf}$ means that cooling can become important even in winds that are too low density to have significant absorption. As such, winds with adiabatic shocks are always optically thin, whereas shocks in optically thick winds are always radiative. Moreover, as detailed in Section 3, even in the bulk of O-star winds for which X-ray absorption is weak or marginal, the structure of X-ray emission associated wind shocks should be dominated by radiative cooling.

2.3 Bridging law between radiative and adiabatic limits

Noting that the pre-shock kinetic energy luminosity of the wind is

$$L_w = 2\pi r_s^2 \rho_{\rm ws} V_\infty^3 = \dot{M} V_\infty^2/2\,, \tag{10}$$

we can use (8a) to eliminate the cooling function $\Lambda_{\rm m}$ from (7b), recasting the X-ray luminosity scaling as a 'bridging law' between the radiative and adiabatic shock limits,

$$L_{\rm xs} = f_{\rm xs}\,\frac{9}{16}\,\frac{L_w}{1+\ell_{\rm s}/r_{\rm s}}\,, \tag{11}$$

where $f_{\rm xs} \equiv f_{\rm x}(T_{\rm s})\delta T_{\rm s}/2T_{\rm s}$ is now a *cooling-integrated* shock X-ray fraction.

Note here that the combination of factors multiplying L_w on the right-hand-side of (11) is just the kinetic energy conversion factor introduced in the summary Fig. 1,

$$k_{\rm x} \equiv \frac{9}{16}\,\frac{f_{\rm xs}}{1+\ell_{\rm s}/r_{\rm s}}\,. \tag{12}$$

For high-density, radiative shocks with $\ell_{\rm s} \ll r_{\rm s}$,

$$L_{\rm xs,rad} = f_{\rm xs}\,\frac{9}{16}\,L_w = f_{\rm xs}\,\frac{9}{32}\,\dot{M} V_\infty^2\,. \tag{13}$$

As a physical interpretation, 9/16 is just the fraction of wind kinetic energy that is converted to post-shock heat, which is radiated away before any losses to adiabatic expansion, with the fraction $f_{\rm xs}$ emitted in the X-ray bandpass of interest. Note that this scales *linearly* with density and thus mass-loss rate, showing that a standard density-squared emission measure does *not* represent an appropriate scaling for emission from radiative shocks.

For lower density, adiabatic shocks with $\ell_{\rm s} \gg r_{\rm s}$, this X-ray emission is reduced by the ratio $r_{\rm s}/\ell_{\rm s}$, giving the scalings,

$$L_{\rm xs,ad} = f_{\rm xs}\,\frac{9}{16}\,\frac{r_{\rm s}}{\ell_{\rm s}}\,L_w \tag{14a}$$

$$= f_{\rm xs}\,\frac{9\pi}{8}\,r_{\rm s}^3 V_\infty^3 \kappa_{\rm cs}\rho_{\rm ws}^2 \tag{14b}$$

$$= f_{\rm xs}\,48\pi r_{\rm s}^3 \Lambda_{\rm m}(T_{\rm s})\rho_{\rm ws}^2 \tag{14c}$$

$$= f_{\rm xs}\,\frac{3\Lambda_{\rm m}(T_{\rm s})}{\pi r_{\rm s}}\left(\frac{\dot{M}}{V_\infty}\right)^2\,, \tag{14d}$$

which thus recovers the density-squared scaling for X-ray luminosity, showing that emission measure does provide an appropriate scaling for emission from adiabatic shocks.

Finally, note that the general bridging law (11) can alternatively be written as a modification of either the radiative or adiabatic scaling,

$$L_{\rm xs} = \frac{L_{\rm xm,rad}}{1+\ell_{\rm s}/r_{\rm s}} \tag{15a}$$

$$= \frac{L_{\rm xm,ad}}{1+r_{\rm s}/\ell_{\rm s}}\,. \tag{15b}$$

This shows that the X-ray luminosity is always limited to be somewhat *below* the *smaller* of the radiative or adiabatic luminosities, i.e. $L_{\rm xs} \lesssim \min(L_{\rm xm,\,rad}, L_{\rm xm,\,ad})$.

2.4 Local X-ray emissivity

To facilitate application of these single standing-shock scalings to the more complex case of multiple embedded wind shocks generated from the LDI, let us next recast these results in terms of the local X-ray emission from an individual shock. Since X-ray emission arises from collision of ions and electrons, it is common to write the X-ray emissivity (per unit volume and solid angle) as scaling with the square of the local density,

$$\eta_{\rm x} = C_{\rm s} f_{\rm v} \rho^2\,, \tag{16}$$

where $C_{\rm s}$ is a constant that depends on the shock strength and atomic physics, and $f_{\rm v}$ represents a local volume filling factor for shocked gas that is sufficiently hot to emit X-rays. If each *individual* shock has an associated filling factor $f_{\rm vs}$ proportional to its post-shock cooling length, then the total filling factor from an *ensemble* of shocks can be written as

$$f_{\rm v}(r) = f_{\rm vs}\,\frac{{\rm d}N_s}{{\rm d}\ln r} = f_{\rm vs}\,n_{\rm s}(r)\,, \tag{17}$$

where $N_s(r)$ is the *cumulative* number of shocks up to radius r, and $n_{\rm s}$ measures the local *differential* number of new, emerging shocks. This formalism emphasizes the importance of the number of shocks and their spatial distribution; compared to the traditional emission measure approach, it should provide more physically motivated constraints for wind-shock X-ray production in massive stars.

In particular, the analysis below of multiple, instability-generated shocks assumes a power-law scaling for $n_{\rm s}$ (see equation 25); but for the above single-shock model, this just takes the form of a Dirac delta-function, $n_{\rm s} = r\delta(r - r_{\rm s})$. The associated X-ray luminosity is then given by integration of the emissivity $\eta_{\rm x}$ over solid angle and volume,

$$L_{\rm x} = 16\pi^2 \int C_{\rm s} f_{\rm vs}\, r\delta(r - r_{\rm s})\rho^2 r^2\,{\rm d}r\,. \tag{18}$$

Upon trivial evaluation over the delta function, comparison with the scalings (14c) and (15b) yields the identifications,

$$C_{\rm s} = \frac{3}{\pi}\Lambda_{\rm m}(T_{\rm s}) f_{\rm xs} \tag{19}$$

and

$$f_{\rm vs} = \frac{1}{1+r_{\rm s}/\ell_{\rm s}}\,. \tag{20}$$

This thus now sets a bridging law at the level of an individual shock, with $f_{\rm vs}$ characterizing the fraction of single-shock emission measure that actually contributes to radiative emission. The adiabatic limit $\ell_{\rm s} \gg r_{\rm s}$ gives $f_{\rm vs} \approx 1$ and so a density-squared scaling for the emissivity (16); the radiative limit reduces this by the small factor

$\ell_s/r_s \ll 1$, thus giving this emissivity a linear-density scaling set by the total kinetic energy flux through the shock.

Note that the factor C_s depends only on the shock strength (through the post-shock temperature T_s), while the shock filling factor f_{vs} depends on the local shock radius and cooling length, as set by the pre-shock wind density. Thus, although these scalings are derived from a simple model of a single, standing shock, they should also be generally applicable to more complex, moving shock structures, if specified in terms of the pre-shock wind density[6] and the relative velocity jump that sets the shock strength and temperature.

3 X-RAYS FROM INSTABILITY-GENERATED EMBEDDED WIND SHOCKS

3.1 Exospheric scaling for L_x

To model the X-ray emission from multiple, embedded wind shocks, let us next write the X-ray luminosity in a fully general, 3D form that accounts for possible directional dependencies in emission and absorption,

$$L_x = \int d^3r \int d\Omega\, \eta_x(\boldsymbol{r}, \boldsymbol{n})\, e^{-\tau(\boldsymbol{r},\boldsymbol{n})}\,, \tag{21}$$

where the optical depth $\tau(\boldsymbol{r}, \boldsymbol{n})$ accounts for bound-free absorption of X-rays emitted at location $\boldsymbol{r}$ in the observer direction $\boldsymbol{n}$.

In principle, instability-generated, X-ray emitting shocks will be associated with a complex, 3D, stochastic wind structure (Dessart & Owocki 2003). But upon averaging over small scales, this can be reasonably well described by a globally spherical wind emission model (OC99). In modelling line emission, accounting for the observed Doppler shift from wind expansion still requires including a directional dependence of the emissivity and optical depth; see Section 4 and Owocki & Cohen (2001, hereafter OC01). But to derive the general scalings for the X-ray luminosity, one can again take the total X-ray emissivity to be an *isotropic* function of the local radius, $\eta_x(r)$. Moreover, given the weak to moderate importance of absorption in all but the densest winds, its overall role in scaling relations can be roughly taken into account through a simple *exospheric* approximation (OC99; Leutenegger et al. 2010), for which the integrations over solid angle and volume in (21) reduce to just a single integration in radius,

$$L_x \approx 16\pi^2 \int_{R_i}^{\infty} \eta_x(r)\, r^2\, dr, \tag{22}$$

where the integral lower bound is taken from the *larger* of the X-ray onset radius and the radius for unit radial optical depth, i.e. $R_i \equiv \max[R_o, R_1]$. For a wind with mass-loss rate $\dot{M}$ and flow speed V_∞, this radius for transition from optically thick to thin X-ray emission is given by

$$R_1 \equiv \tau_* R_* = \frac{\kappa_{bf}\dot{M}}{4\pi V_\infty} \approx 25\,R_\odot\, \frac{\dot{M}_{-6}}{E_{kev}^2 V_{1000}}\,, \tag{23}$$

where τ_* is a characteristic wind optical depth to the stellar surface radius R_*, and the latter equalities use the scaling (9) for the bound-free X-ray opacity κ_{bf}, with $\dot{M}_{-6} \equiv \dot{M}/(10^{-6}\,M_\odot\,yr^{-1})$ and $V_{1000} \equiv V_\infty/1000\,km\,s^{-1}$.

[6] For instability-generated wind structure, X-rays can arise from collisions between clumps that have been compressed to some fraction of the wind volume (Feldmeier et al. 1997b), implying then a higher input density that would lower the cooling length. For simplicity, the analysis here does not account for this possibility, but it could enhance the importance of radiative cooling, leading to an even larger effective ratio κ_{cs}/κ_{bf} of cooling to absorption.

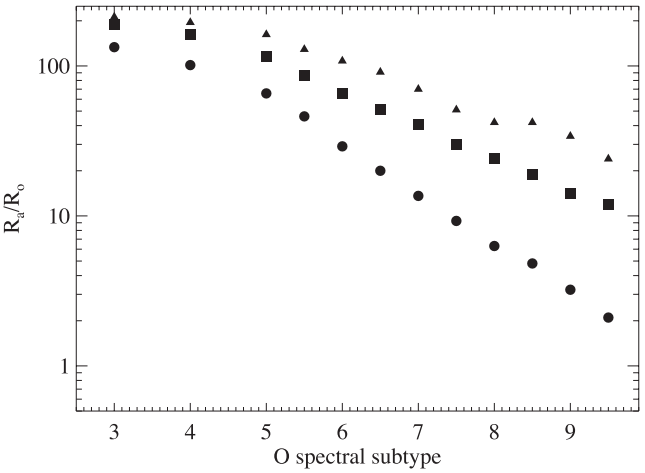

Figure 2. Ratio R_a/R_o of adiabatic radius to shock onset radius, assuming $R_o = 1.5R_*$, and a post-shock temperature $T_{kev} = 0.5$. To construct the plot, stellar parameters were taken from tables 1– 3 of Martins et al. (2005) (T_{eff}, L_{bol}, R_*, M_*) for luminosity classes V, III and I (marked, respectively, by circles, squares and triangles). The terminal speeds are computed as $V_\infty = 2.6V_{esc}$, and mass-loss rates are from Vink, de Koter & Lamers (2000).

In direct analogy, we can similarly define a characteristic *adiabatic radius* for transition from radiative to adiabatic cooling of the associated wind shocks,

$$R_a \equiv \frac{\kappa_{cs}\dot{M}}{4\pi V_\infty} \approx 625\,R_\odot\, \frac{\dot{M}_{-6}}{T_{kev}^2 V_{1000}}\,, \tag{24}$$

where $T_{kev} = kT_s/keV$. For X-rays emitted with photon energy comparable to the shock energy, $E_{kev} \approx T_{kev}$, we find $R_a/R_1 \approx \kappa_{cs}/\kappa_{bf} \approx 25$. As detailed below, this implies there can be extensive wind regions in which the density is high enough for shocks to be radiative, but too low for much wind absorption of their emitted X-rays. In particular, independent of the mass-loss rate, any shocks formed near the radius R_1, where X-rays have near unit optical depth, should always be strongly radiative.

Fig. 2 plots estimates of R_a/R_o versus O-star spectral subtype, for shocks with the temperature $T_{kev} = 0.5$, as expected for wind shocks generated by the LDI (Runacres & Owocki 2002; Dessart & Owocki 2003), and estimated from the observed, relatively soft X-ray spectra (Wojdowski & Schulz 2005; Zhekov & Palla 2007; Nazé, Flores & Rauw 2012). The large R_a values confirm that wind shocks of this energy should be radiative.

This plot can also be readily used to estimate expected unit optical depth radii. In particular, for an emission line at $E_{kev} = 1$, the corresponding R_1 would be a factor of 100 smaller than the R_a plotted in Fig. 2. Since this means most O-stars would have $R_1/R_o \lesssim 1$, we see that absorption effects should be weak to moderate throughout the O-star domain, even while the shocks are generally radiative. See Section 5 and Fig. 4 for further discussion and illustration of these scalings.

3.2 Bridging law with thin-shell mixing

Previous analyses using the density-squared emissivity (16) (e.g. OC99; OC01) have directly parametrized the X-ray filling factor f_v as following some specified radial function, e.g. a power law.

But instead let us now parametrize the shock-*number* distribution in (17) by an analogous power law,

$$n_s(r) \equiv n_{so} \left(\frac{R_o}{r} \right)^p \quad ; \quad r > R_o \,, \tag{25}$$

with $n_s = 0$ for $r < R_o$. Both instability simulations (Owocki & Puls 1999; Runacres & Owocki 2002; Dessart & Owocki 2003) and X-ray profile fitting and He-like f/i ratios (Cohen et al. 2006, 2010, 2011; Leutenegger et al. 2006) suggest an initial onset for shock formation around $R_o \approx 1.5 R_*$.

Applying (25) in (17), the analysis in Section 2.4 provides a more physical model of shock X-ray emission that accounts explicitly for the effects of radiative cooling. However, it still does not account for any thin-shell *mixing*. The inherent thinness ($\ell \ll r$) of radiative shock cooling zones makes them subject to various thin-shell instabilities (Vishniac 1994), which in numerical simulations lead to highly complex, turbulent shock structure (e.g. Walder & Folini 1998). Parkin & Pittard (2010) discuss how the inherently limited spatial resolution of radiative shock simulations leads to a 'numerical conduction' that transports heat from high- to low-temperature gas, resulting in a severe, but difficult-to-quantify reduction in the X-ray emission.

While the specific mechanisms within hydrodynamical simulations may indeed depend on such *numerical* artefacts, the perspective advocated here is that such an overall reduction in X-ray emission is likely a natural consequence of the turbulent cascade induced by the thin-shell instability; this should lead to substantial *physical* mixing between cool and hot material, with the softer and more efficient radiation of the cooler gas effectively reducing the emission in the X-ray bandpass.

Pending further simulation studies to quantify such mixing and X-ray reduction, we make here the plausible ansatz that the reduction should, for shocks in the radiative limit $\ell/r \ll 1$, scale as some power m of the cooling length ratio, $(\ell/r)^m$. To ensure that the mixing becomes ineffective in the adiabatic limit – for which the cooling layer is too extended to be subject to thin-shell instability – we recast the bridging law (20) for the shock volume filling factor f_{vs} in the generalized form,

$$f_{vs} \approx \frac{1}{(1 + r/\ell)^{1+m}} = \frac{1}{(1 + \kappa_c \rho r)^{1+m}} \,, \tag{26}$$

with the level of mixing now controlled by a positive value of the mixing exponent m. To simplify notation in the analysis to follow, we have dropped here the subscripts ('s' or 'w') for the quantities (e.g. ℓ, r, κ_c, ρ) on the right-hand-side. Recalling that the cooling coefficient κ_c takes the scalings given in equations (8a)–(8c), we can use the adiabatic radius R_a from (24) to characterize the asymptotic regimes for (26).

If $R_a < R_o$, then the shocks are adiabatic throughout the wind, and we recover the standard density-squared emissivity (16) with a specified volume filling factor set by $f_v = n_s$.

If $R_a > R_o$, this adiabatic scaling still applies in the outer wind, $r > R_a$; but in the inner regions $R_o < r < R_a$, the cooling term in the denominator of (26) dominates, giving the emissivity (16) now a *reduced* dependence on density,

$$\eta_x \approx C_s n_s \frac{\rho^{1-m}}{(\kappa_c r)^{1+m}} \quad ; \quad R_o < r < R_a \,. \tag{27}$$

Without mixing ($m = 0$), the density dependence is thus linear, but with mixing ($m > 0$), it becomes *sub-linear*.

As noted above, absorption is a modest effect in even dense O-star winds, with $\tau_* $ at most of the order of unity, implying then that $R_1 \lesssim R_o$ (Cohen et al. 2010). But the stronger coefficient ($\kappa_c/\kappa_{bf} = R_a/R_1 \approx 25$) for radiative cooling means that such winds typically have $R_a > R_o$, implying that most shocks remain radiative well above the wind acceleration region where they are generated.

3.3 L_x scalings with $\dot{M}/V_\infty$

Let us now turn to the scalings for the overall X-ray luminosity. Applying the emissivity (16) and filling factor (26) to the exospheric model (22) with the power-law shock distribution (25), we find

$$\begin{aligned} L_x &\approx 16\pi^2 C_s \int_{R_i}^{\infty} \frac{n_s \rho^2}{(1 + \kappa_c \rho r)^{1+m}} \, r^2 \, dr \\ &= C_p \left[\frac{\dot{M}}{V_\infty} \right]^2 \int_{R_i}^{\infty} \frac{dr}{r^p (rw)^{1-m} (rw + R_a)^{1+m}} \,, \end{aligned} \tag{28}$$

where $C_p \equiv C_s n_{so} R_o^p$ and the latter equality uses mass conservation to cast the integral in terms of the scaled wind velocity, $w(r) \equiv v(r)/V_\infty$. This is generally taken to have a 'beta-law' form $w(r) = (1 - R_*/r)^\beta$, with the canonical case $\beta = 1$ giving $rw = r - R_*$, and the constant-speed case $\beta = 0$ giving $rw = r$. For these special cases, Section 5 gives some results for full integrations of (28).

But even for a generic velocity law $w(r)$, we can readily glean the essential scalings of the L_x from (28) in key asymptotic limits of adiabatic versus radiative shocks.

3.3.1 *Adiabatic shocks in optically thin wind*

First, for low-density winds with optically thin emission from adiabatic shocks, $R_1 < R_a < R_o$, we can effectively drop the R_a term in the denominator, and set the lower bound of the integral to the fixed onset radius, $R_i = R_o$, yielding

$$L_x \approx C_p \left[\frac{\dot{M}}{V_\infty} \right]^2 \int_{R_o}^{\infty} \frac{dr}{w^2 r^{p+2}} \quad ; \quad R_1 < R_a < R_o \,. \tag{29}$$

Since the resulting integral then is just a fixed constant that is independent of $\dot{M}$, the X-ray luminosity recovers the standard adiabatic scaling $L_x \sim (\dot{M}/V_\infty)^2$.

3.3.2 *Radiative shocks in optically thin or thick wind*

For high-density winds with radiative shocks and so $R_o < R_a$, the R_a now dominates its term, and so can be pulled outside the integral. Rescaling the remaining integrand in terms of the initial radius R_i, we find

$$L_x = C_p \left[\frac{\dot{M}}{V_\infty} \right]^2 \frac{R_i^{m-p}}{R_a^{m+1}} \int_1^{\infty} \frac{dr}{r^p (rw)^{1-m}} \quad ; \quad R_o < R_a \,, \tag{30}$$

where again the integral is now essentially independent of $\dot{M}/V_\infty$.

For the intermediate-density case in which the radiative shock emission is optically thin, $R_1 < R_o < R_a$, the integration lower limit is fixed at the onset radius, $R_i = R_o$, which is independent of $\dot{M}/V_\infty$. But since $R_a \sim \dot{M}/V_\infty$, the overall scaling is $L_x \sim (\dot{M}/V_\infty)^{1-m}$.

For the case of very dense, optically thick winds with radiative shocks, $R_o < R_1 < R_a$, the lower boundary at $R_i = R_1$ gives the residual integral an additional dependence on R_1^{m-p}; since R_1 too scales with mass-loss rate, the dependence on the mixing index m *cancels*. At the radius R_1 the cooling length ratio ℓ/r is always the same, implying that in optically thick winds the observed radiative shock emission is likewise fixed for any mass-loss rate. The luminosity scaling thus becomes *independent* of mixing, scaling just with shock-number index as $L_x \sim (\dot{M}/V_\infty)^{1-p}$.

This is in fact the same scaling found in OC99 for optically thick winds, but with *adiabatic* shocks. Indeed, OC99 argued that assuming a filling factor $f_v \sim r^{-0.4}$ could give a sub-linear dependence on mass-loss rate, $L_x \sim \dot{M}^{0.6}$, and so possibly reproduce the $L_x \sim L_{bol}$ relation. Subsequent analysis of X-ray line profiles observed from *Chandra* and *XMM–Newton* have shown, however, that optical depth effects are quite moderate even for O-stars like ζ Puppis with quite dense winds (Cohen et al. 2010). The bulk of O-star winds are simply too low density for this optical thickness scaling to apply, and so this cannot be the explanation for the $L_x \sim L_{bol}$ relation.

3.3.3 *Summary of asymptotic scalings*

To summarize, power-law shock-number models with thin-shell mixing have the asymptotic scalings,

$$L_x \sim \left[\frac{\dot{M}}{V_\infty}\right]^2 \quad ; \; R_1 < R_a < R_o \; ; \text{ adiabatic, thin} \tag{31a}$$

$$\sim \left[\frac{\dot{M}}{V_\infty}\right]^{1-m} \quad ; \; R_1 < R_o < R_a \; ; \text{ radiative, thin} \tag{31b}$$

$$\sim \left[\frac{\dot{M}}{V_\infty}\right]^{1-p} \quad ; \; R_o < R_1 < R_a \; ; \text{ radiative, thick,} \tag{31c}$$

where the progression represents a trend of increasing $\dot{M}/V_\infty$. The first applies for weak winds, for example from early B main-sequence stars, which typically show weak X-ray emission, with L_x well below $10^{-7} L_{bol}$ (Cohen et al. 1997). The middle scaling for intermediate-density winds is the most relevant for the bulk of O-type stars found to follow the $L_x \sim L_{bol}$ relation. The last applies only to the strongest winds, e.g. very early O supergiants like HD93129A, for which analysis of X-ray line profiles show moderate absorption effects,[7] with $\tau_* \gtrsim 1$ (Cohen et al. 2011).

3.4 Link between $\dot{M}$ and L_{bol} scaling

As noted in the introduction, and summarized in Fig. 1, straightforward application of CAK wind theory implies a *direct* dependence of mass-loss rate on luminosity that scales as $\dot{M} \sim L_{bol}^{1/\alpha}$, where $\alpha \approx 0.6$ is the CAK power index; for the bulk of O-type stars with intermediate-density winds and thus $L_x \sim \dot{M}^{1-m}$, reproducing the observed $L_x \sim L_{bol}$ relation thus simply requires a mixing exponent $m \approx 1 - \alpha \approx 0.4$.

More generally, let us now consider how this requirement is affected if one accounts also for a secondary dependence on stellar mass M, which in turn can give a further *indirect* dependence on L_{bol}. Specifically, within CAK wind theory, $\dot{M} \sim M^{1-1/\alpha}$ and $V_\infty \sim M^{1/2}$, and so if we in turn assume from stellar structure a mass–luminosity dependence $M \sim L_{bol}^s$, where $s \approx 1/3$ (e.g. Maeder 2009, p. 360), we find

$$\log\left(\frac{\dot{M}}{V_\infty}\right) \sim \frac{2 - s(2-\alpha)}{2\alpha} \log(L_{bol}) \sim \frac{\log(L_x)}{1-m}, \tag{32}$$

where the latter relation makes use of the scaling (31b).[8]

[7] Indeed, this star could be viewed as a transitional object to the WNH-type Wolf–Rayet stars, for which absorption effects should strongly attenuate any X-rays from instabilities in the wind acceleration region; see Section 6.

[8] Of course, the terminal speed also depends on stellar radius as $V_\infty \sim 1/\sqrt{R_*}$, but the diverse luminosity classes of X-ray emitting O-stars makes it difficult to identify any *systematic* dependence on L_{bol} that might influence the overall $L_x - L_{bol}$ relation.

Reproducing the empirical $L_x \sim L_{bol}$ relation thus now requires

$$m = \frac{2(1-\alpha) - s(2-\alpha)}{2 - s(2-\alpha)}. \tag{33}$$

Accounting for a stellar structure scaling $s \approx 1/3$ with a CAK index $\alpha \approx 0.6$ thus now requires a mixing exponent $m \approx 0.22$, somewhat smaller than the $m \approx 0.4$ required if one assumes no systematic mass–luminosity scaling (i.e. $s = 0$).

4 EFFECT OF SHOCK COOLING ON X-RAY LINE PROFILES

4.1 Basic formalism

Observations by *XMM–Newton* and *Chandra* of spectrally resolved, wind-broadened X-ray emission lines from luminous OB stars provide a key diagnostic of the spatial distribution of X-ray emission and absorption in their expanding stellar winds (Ignace & Gayley 2002; Oskinova, Feldmeier & Hamann 2006; Owocki & Cohen 2006). In particular, the relatively weak blue–red asymmetry of the observed emission lines indicates modest wind optical depths, $\tau_* \sim 1$, while the overall width constrains the spatial location of the emission within the expanding velocity law. For the usual density-squared emission model with a prescribed (power law) spatial variation in volume filling factor f_v, fits to observed X-ray lines are typically consistent with a standard $\beta \approx 1$ velocity law and an f_v that is spatially nearly *constant*, corresponding to $p \approx 0$ within the adiabatic scaling implicit in the emission measure analysis (Kramer, Cohen & Owocki 2003; Cohen et al. 2006). In the discussion below, we refer to these profiles – plotted in black in Fig. 3 – as 'observationally favoured'.

Within the perspective discussed here that shocks within most O-star winds are likely to be radiative instead of adiabatic, let us

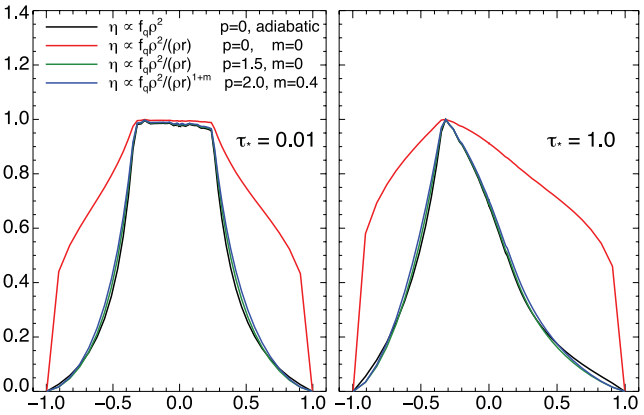

Figure 3. X-ray line profiles (normalized to unit maximum) versus Doppler-shifted wavelength (normalized to shift for terminal velocity V_∞), for optically thin ($\tau_* \ll 1$; left) and marginally optically thick ($\tau_* = 1$; right) lines. The black curves show the adiabatic, constant-filling-factor models that give good general fits to observed X-ray emission lines. The other curves show radiative models for no mixing and for $m = 0.4$, with shock-number indices p as labelled. Radiative models with constant shock number ($p = 0$) give profiles that are too broad (red curves). But models with steeper number exponents ($p = 1.5$ for $m = 0$ in green; and $p = 2$ for $m = 0.4$ in blue) fit well the observationally favoured black curves. If the O-star $L_x - L_{bol}$ relation is to be reproduced with moderate thin-shell mixing ($m \approx 0.4$) of radiative shocks, then matching observed X-ray emission lines requires the shock number to have a moderately steep decline ($p \approx 2$) above the initial onset radius R_o.

now examine how inclusion of radiative cooling affects X-ray line profiles. Following OC01, the directional Doppler shift of the X-ray line emission within the expanding wind is modelled through a line emissivity $\eta_\lambda(r, \mu)$ at an observer's wavelength λ along direction cosine μ from a radius r. The resulting X-ray luminosity spectrum L_λ is computed from integrals of the emission over direction and radius, attenuated by bound-free absorption within the wind (cf. OC01, equation 1),

$$L_\lambda = 8\pi^2 \int_{-1}^{1} \mathrm{d}\mu \int_{R_*}^{\infty} \mathrm{d}r\, r^2 \eta_\lambda(\mu, r)\, \mathrm{e}^{-\tau(\mu,r)}. \tag{34}$$

The absorption optical depth $\tau(\mu, r)$ is evaluated by converting to ray coordinates and then integrating for each ray with a fixed impact parameter from the local position to the observer. For the standard $\beta = 1$ velocity law, the integrals are analytic, with overall scaling in proportion to $\tau_* \equiv R_1/R_*$.

In principle, this integrated optical depth can be affected by the 'porosity' associated with optically thick clumps or anisotropic 'pancakes' (Feldmeier, Oskinova & Hamann 2003), with potential consequences for interpreting the *asymmetry* of X-ray line profiles in terms of the wind mass-loss rate (Oskinova et al. 2006). But for the optically thin ($\tau_* \ll 1$) or marginally optically thick ($\tau_* \sim 1$) lines considered here, individual clumps should be optically thin (Owocki & Cohen 2006; Sundqvist et al. 2012), and so such effects are not important for the discussion below, which focuses on the overall profile width.

4.2 Scaling analysis

As noted, applications of this OC01 formalism assuming a density-squared emission show that a spatially constant X-ray volume filling factor f_v gives generally quite good fits to observed X-ray lines. To examine the effect of radiative cooling, let us now apply the more general bridging-law scalings of (16) and (26), assuming the simple power-law form for the shock number (25). The spatial integration thus takes the same form as the exospheric result (28), except that absorption is now treated explicitly by the exponential optical depth term in the integrand, with the radial lower bound fixed at the X-ray onset radius, $R_i = R_o$.

We can again infer basic scaling results by inspection of this integrand in the limits of adiabatic versus radiative shocks. For the adiabatic case, this follows the scaling in (29), with radial dependence $1/w^2 r^{p+2}$. To match observed profiles, such adiabatic emission models require constant $f_v = n_s$, with the zero power-law exponent $p = 0$ implying a $1/(wr)^2$ variation of the integrand.

By contrast, the radiative limit follows the scaling in (30), with direct radius dependence $1/r^{p+1-m}$, and velocity dependence $1/w^{1-m}$ that is weaker than the $1/w^2$ of the adiabatic model. Focusing first just on the former, we see that reproducing the $1/r^2$ integrand needed to fit observed profiles would now require $p = 1 + m$. In practice, to compensate for the weaker inverse-speed dependence, fitting the observed profile width requires a somewhat steeper shock-number decline, as we now quantify.

4.3 X-ray line profiles from radiative shocks

For a $\beta = 1$ velocity law with $R_o = 1.5R_*$ and various specified values of the exponents p and m, Fig. 3 plots normalized X-ray line profiles for optically thin ($\tau_* \ll 1$; left) and marginally optically thick ($\tau_* = 1$; right) lines. In both cases, the black curve represents the adiabatic, constant-filling-factor ($p = 0$) model that gives generally good fits to observed profiles.

The other curves show results for radiative shocks. Without mixing, the red curve for radiative shocks with constant shock number ($p = 0$) is far too broad; fitting the favoured black profile now requires a $p = 1.5$ (blue curve), which is even steeper than the predicted $p = m + 1 = 1$ needed to compensate for the weaker direct radial scaling. With mixing exponent of $m = 0.4$, we find that a $p = 1.5$ shock-number model gives profiles (not shown) that are still somewhat too broad. But with a somewhat steeper number exponent $p = 2$, the blue curve again nearly reproduces the black curve.[9]

An overall conclusion is thus that, for radiative shock models with mixing at a level needed to reproduce the $L_x \sim L_{bol}$ relation, matching observed X-ray emission requires a steep radial decline ($p \approx 2$) in shock number above the onset radius.

4.4 Decline of L_x in optically thick winds

Such a steep radial drop off in shock number has important implications for the scaling of X-ray luminosity for the highest density stars that become optically thick to bound-free absorption, i.e. with $\tau_* > 1$ and thus $R_1 > R_o$. Namely, from the scaling given by (31c), we see that taking $p \approx 2$ implies that the X-ray luminosity for such optically thick winds should now *decline inversely* with mass-loss rate, $L_x \sim \dot{M}^{1-p} \sim 1/\dot{M}$. If the X-ray emission is concentrated near an onset radius within the wind acceleration zone, the bound-free absorption by the overlying, optically thick wind significantly attenuates the net X-rays seen by an external observer. For early O-type supergiants with dense winds, this can lead to a reduced X-ray luminosity, but because the overall decline of bound-free opacity with X-ray energy, the observed spectrum can be hardened. The recent analysis of X-rays from the O2If star HD 93129A provides a potential example approaching this limit (Cohen et al. 2011).

5 SCALING RESULTS FOR FULL EVALUATION OF L_x INTEGRAL

5.1 Constant-speed wind with $\beta = 0$

As a supplement to the asymptotic L_x scalings given in Section 3.3, let us finally consider full solutions for the general integral (28). For a constant speed model with $\beta = 0$ and thus $w(r) = 1$, general analytic integration is possible in terms of the incomplete beta function. But the typical properties can be more simply gleaned by examining the special case $p = 1$, for which the integral in (28) takes the simpler analytic form,

$$L_x = \frac{C_p p \kappa_c^2}{16\pi^2 m(1-m)} \left[\frac{1 + m R_a/R_i}{(1 + R_a/R_i)^m} - 1 \right], \tag{35}$$

wherein the square-bracket factor sets the scalings with $\dot{M}/V_\infty$, with the preceding terms just fixing the overall normalization. For low-density, optically thin winds, the initial radius is fixed to the onset radius, so that $R_a/R_i \sim R_a/R_o \sim \dot{M}/V_\infty$. For $R_a/R_o \ll 1$, expansion of the square-bracket term recovers the adiabatic scaling $L_x \sim (\dot{M}/V_\infty)^2$ of (31a), while for $R_a/R_o \gg 1$, it becomes proportional to R_a^{1-m} and so recovers the radiative, optically thin scaling (31b). For high-density, optically thick winds, the ratio

[9] Also not shown here are profiles computed for $p = 2$ and the alternative mixing exponent value $m = 0.22$, which we find also give close agreement with the black curves.

$R_a/R_i = R_a/R_1$ becomes independent of mass-loss rate, and so the square-bracket factor and thus L_x approach a constant value, in accord with (31c) for this case with $p = 1$.

5.2 Standard wind with $\beta = 1$

For a standard $\beta = 1$ velocity law with $rw = r - R_*$, analytic integration of (28) can be cast in terms of the Appell hypergeometric function; but in practice it is more straightforward just to carry out the integration numerically.

Fig. 4 plots the resulting X-ray luminosity L_x [scaled by the dimensional factor outside the square brackets in (35)] versus adiabatic radius R_a (scaled by the shock-onset radius R_o), as computed from numerical integration of (28) for the selected, labelled values of the mixing exponent m and shock-number exponent p. As seen from (24), plotting versus R_a can be viewed as a proxy for plotting versus the wind density parameter $\dot{M}/V_\infty$.

The left vertical line at $R_a/R_o = 1$ represents the transition from low-density adiabatic shocks, for which $L_x \sim \dot{M}^2$, to intermediate-density radiative shocks, for which $L_x \sim \dot{M}^{1-m}$.

The right vertical line represents the transition from optically thin to thick winds, implemented here through a sudden change in the integration lower bound, $R_i = \max(R_1, R_o)$, with the shock onset radius fixed at $R_o = 1.5R_*$, and R_1 the radius for unit optical depth. Like R_a, R_1 scales with $\dot{M}/V_\infty$, with values that are a small, fixed fraction $R_1/R_a \equiv f_{1a}$ of the adiabatic radius. Since observed X-rays are typically a modest factor higher energy than the characteristic wind shock (e.g. $E_{kev} \approx 1 \approx 2T_{kev}$), the curves plotted in Fig. 4 assume, following (23) and (24), $f_{1a} = R_1/R_a = \kappa_{bf}/\kappa_c \approx 1/100$. For very large $R_a > R_o/f_{1a} \approx 100R_o$, we thus have $R_1 > R_o$, leading to a declining L_x, as predicted by the optically thick wind scaling $L_x \sim R_a^{1-p}$ from (31c).

But for moderately dense winds, with $R_o < R_a < R_o/f_{1s}$ (between the vertical lines in the figure), the increasing L_x approaches the power-law variation R_a^{1-m} predicted by (31b). In particular, the black curve with $p = 2$ and $m = 0.4$ represents the preferred model with sub-linear scaling in R_a, and thus in $\dot{M}/V_\infty$, implying a nearly linear scaling of L_x with L_{bol}.

Specifically, for typical values for stellar radius ($R_* \approx 10-20\,R_\odot$) and wind terminal speed ($V_\infty \approx 2000\,km\,s^{-1}$), this intermediate-density regime with $L_x \sim L_{bol}$ applies to wind mass-loss rates that range from below $10^{-7}\,M_\odot\,yr^{-1}$ to a few times $10^{-6}\,M_\odot\,yr^{-1}$; this essentially encompasses the entire O-star spectral range for which the $L_x \sim 10^{-7}L_{bol}$ relation is found to hold.

6 CONCLUDING SUMMARY

The central result of this paper is that, in the common case of moderately dense O-star winds with radiative shocks ($R_a > R_o$), thin-shell mixing can lead to this *sub-linear* scaling of the X-ray luminosity with the mass-loss rate, $L_x \sim (\dot{M}/V_\infty)^{1-m}$. Depending on the secondary scalings of wind density with bolometric luminosity, one finds that $m \approx 0.2-0.4$ can give roughly the *linear* L_x–L_{bol} law that is empirically observed for O-star X-rays. Further simulation work will be needed to see if such mixing exponent values are

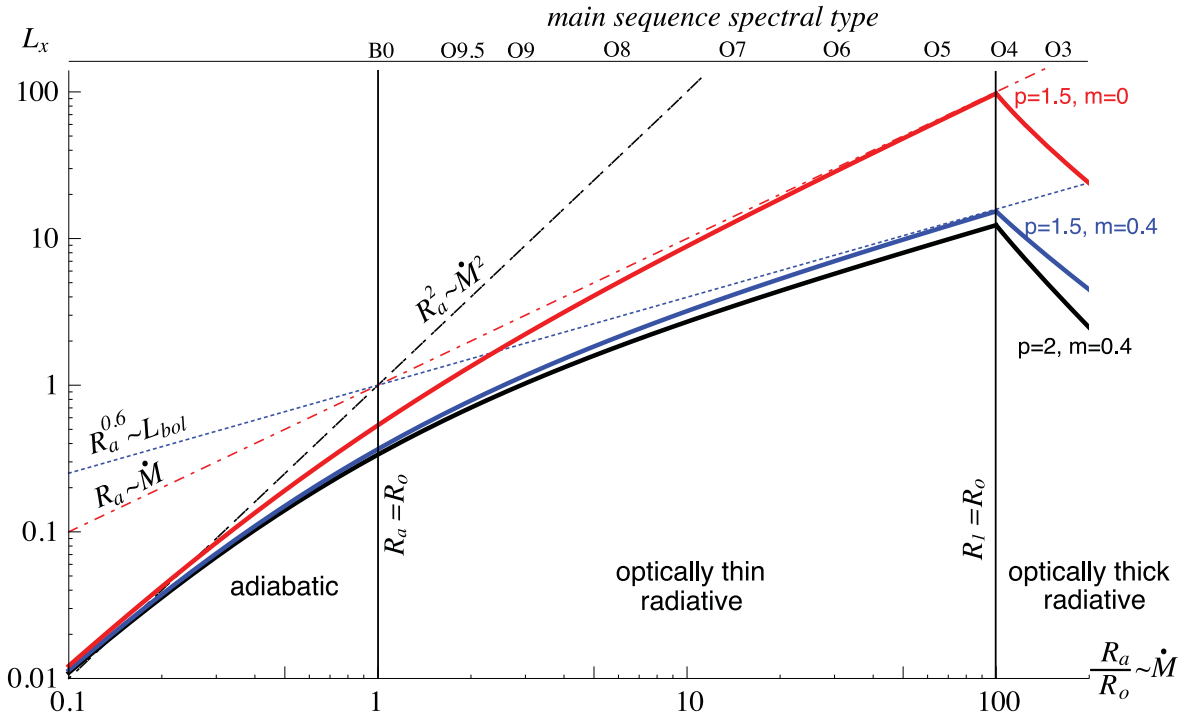

Figure 4. Normalized X-ray luminosity L_x versus adiabatic radius R_a scaled by shock onset radius $R_o = 1.5R_*$, for winds with a standard $\beta = 1$ velocity law, and selected, labelled values for the parameters p and m. The dashed, dot–dashed and dotted lines show the expected scalings for, respectively, adiabatic, radiative and thin-shell-mixed shocks. As discussed in the text, the variation in R_a represents a proxy for the wind density parameter $\dot{M}/V_\infty$, ranging from low-density, adiabatic shocks on the far left, to high-density, optically thick winds with radiative shocks on the far right; the optically thick turnover at $R_a/R_o > 100$ applies for observed X-ray energies that are about a factor of 2 higher than the shock energy. The intermediate-density case with optically thin, radiative shocks follows the $L_x \sim \dot{M}^{1-m}$ scaling that reproduces the empirical $L_x \sim L_{bol}$ relation if $m \approx 0.4$. The upper axis uses the analysis from Fig. 2 to mark the corresponding spectral class for main sequence stars; for higher luminosity giants and supergiants, the associated spectral class sequence would shift to the right.

appropriate, and indeed to test the validity of the basic mixing exponent ansatz.

But in the course of exploring this idea of thin shell mixing, the analysis here has lead to several interesting secondary results with validity and implications that are largely independent of mixing or any specific model for it. A summary list includes the following.

(i) In contrast to previous analyses that invoked a density-squared emission measure description for shock production of X-rays, we derive here a more general bridging law showing how the density-squared scaling of adiabatic shocks transitions to a single density scaling for radiative shocks.

(ii) For radiative shocks, the X-ray volume filling factor is not fixed (as is commonly assumed), but is reduced by the narrow extent of the shock layer, $f_v \sim \ell/r$.

(iii) For nearly all O-stars, the large radiative–adiabatic transition radius, $R_a \gg R_o \approx 1.5R_*$, implies that instability-generated shocks in the wind acceleration region should follow the radiative scaling, giving the X-ray luminosity a linear scaling with mass-loss rate, $L_x \sim \dot{M}/V_\infty$.

(iv) For low-density winds of lower luminosity (early B) stars, shocks should indeed become adiabatic, implying then a steep ($L_x \sim \dot{M}^2$) decline of X-ray luminosity, as is in fact generally found for single, non-magnetic, early B-type stars, for which the inferred X-ray emission measure often approaches that of the full wind (Cohen et al. 1997, 2008)

(v) Matching observed X-ray emission lines with such models of radiative shocks with or without thin-shell mixing requires the shock number to have a moderately steep decline above the X-ray onset radius, with power-law exponent $p \approx 1.5-2$.

(vi) This in turn implies that the scaling of X-ray luminosity for dense, optically thick winds should saturate and even decline with increasing mass-loss rate.

This last result on X-ray absorption is perhaps not too relevant for most of the O-stars following the $L_x - L_{bol}$ relation, for which optical depth effects are weak to marginal. But it can become important for the dense, moderately optically thick winds of extreme, early O-stars like HD 93129A, which can be viewed as a transitional object to the WNH-type Wolf–Rayet stars (Smith & Conti 2008). More generally, the high density of Wolf–Rayet winds imply that absorption should strongly attenuate X-rays from any instability-generated shocks in their wind acceleration region. As such, the observed hard X-rays seen from Wolf–Rayet stars like WR6 (EZ CMa) seem unlikely to be explained by this standard model of LDI shocks (Oskinova et al. 2012). This also has potential implications for interpreting observed X-rays from very massive stars that have $L_x \sim 10^{-7}L_{bol}$ despite having very high wind optical depths (Crowther et al. 2010), and whether these might instead originate from wind–wind collisions of close, undetected binary companions.

Indeed, the mixing ansatz in this paper could also be applied to model X-ray emission from CWB, and their L_x scaling with orbital separation. Wide binaries with adiabatic shocks should still follow the usual inverse distance scaling, as directly confirmed by observations of multiyear-period elliptical systems like WR140 and η Carinae (Corcoran 2012). But in close, short (day to week) period binaries with radiative shocks (Antokhin et al. 2004), mixing could reduce and limit the effective X-ray emission from the wind collision (Parkin & Pittard 2010), and thus help clarify why such systems often hardly exceed the $L_x \approx 10^{-7}L_{bol}$ scaling found for single stars (Oskinova 2005; Corcoran 2012; Gagné et al. 2012).

Finally, in addition to exploring such effects in CWB, a top priority for future work should be to carry out detailed simulations of the general effect of thin-shell mixing on X-ray emission, and specifically to examine the validity of this mixing-exponent ansatz for modelling the resulting scalings for X-ray luminosity.

ACKNOWLEDGMENTS

This work was supported in part by NASA ATP grant NNX11AC40G to the University of Delaware. DHC acknowledges support from NASA ADAP grant NNX11AD26G and NASA *Chandra* grant AR2-13001A to Swarthmore College.

REFERENCES

Antokhin I. I., Owocki S. P., Brown J. C., 2004, ApJ, 611, 434
Babel J., Montmerle T., 1997, ApJ, 485, L29
Berghoefer T. W., Schmitt J. H. M. M., Danner R., Cassinelli J. P., 1997, A&A, 322, 167
Castor J. I., Abbott D. C., Klein R. I., 1975, ApJ, 195, 157 (CAK)
Chlebowski T., Harnden F. R. Jr, Sciortino S., 1989, ApJ, 341, 427
Cohen D. H., Cassinelli J. P., Macfarlane J. J., 1997, ApJ, 487, 867
Cohen D. H., Leutenegger M. A., Grizzard K. T., Reed C. L., Kramer R. H., Owocki S. P., 2006, MNRAS, 368, 1905
Cohen D. H., Kuhn M. A., Gagné M., Jensen E. L. N., Miller N. A., 2008, MNRAS, 386, 1855
Cohen D. H., Leutenegger M. A., Wollman E. E., Zsargó J., Hillier D. J., Townsend R. H. D., Owocki S. P., 2010, MNRAS, 405, 2391
Cohen D. H., Gagné M., Leutenegger M. A., MacArthur J. P., Wollman E. E., Sundqvist J. O., Fullerton A. W., Owocki S. P., 2011, MNRAS, 415, 3354
Corcoran M., 2012, in Drissen L., Robert C., St-Louis N., Moffat A., eds., ASP Conference Series, Vol. 465, Four Decades of Research on Massive Stars. Astron. Soc. Pac., San Francisco, p. 330
Crowther P. A., Schnurr O., Hirschi R., Yusof N., Parker R. J., Goodwin S. P., Kassim H. A., 2010, MNRAS, 408, 731
Dessart L., Owocki S. P., 2003, A&A, 406, L1
Feldmeier A., Kudritzki R.-P., Palsa R., Pauldrach A. W. A., Puls J., 1997a, A&A, 320, 899
Feldmeier A., Puls J., Pauldrach A. W. A., 1997b, A&A, 322, 878
Feldmeier A., Oskinova L., Hamann W.-R., 2003, A&A, 403, 217
Gagné M., 2012, in Drissen L., Robert C., St-Louis N., Moffat A., eds., ASP Conference Series, Vol. 465, Four Decades of Research on Massive Stars. Astron. Soc. Pac., San Francisco, p. 301
Güdel M., Nazé Y., 2009, A&AR, 17, 309
Hervé A., Rauw G., Nazé Y., Foster A., 2012, ApJ, 748, 89
Hillier D. J., Kudritzki R. P., Pauldrach A. W., Baade D., Cassinelli J. P., Puls J., Schmitt J. H. M. M., 1993, A&A, 276, 117
Ignace R., Gayley K. G., 2002, ApJ, 568, 954
Kramer R. H., Cohen D. H., Owocki S. P., 2003, ApJ, 592, 532
Krolik J. H., Raymond J. C., 1985, ApJ, 298, 660
Kudritzki R. P., Palsa R., Feldmeier A., Puls J., Pauldrach A. W. A., 1996, in Zimmermann H. U., Trümper J., Yorke H., eds, Roentgenstrahlung from the Universe: The X-ray emission from O stars. Fachinformationszentrum TIB, Karlsruhe, p. 9
Leutenegger M. A., Paerels F. B. S., Kahn S. M., Cohen D. H., 2006, ApJ, 650, 1096
Leutenegger M. A., Cohen D. H., Zsargó J., Martell E. M., MacArthur J. P., Owocki S. P., Gagné M., Hillier D. J., 2010, ApJ, 719, 1767
Maeder A., 2009, Physics, Formation and Evolution of Rotating Stars. Springer, Berlin, Heidelberg
Martins F., Schaerer D., Hillier D. J., Meynadier F., Heydari-Malayeri M., Walborn N. R., 2005, A&A, 441, 735
Nazé Y., 2009, A&A, 506, 1055
Nazé Y. et al., 2011, ApJS, 194, 7
Nazé Y., Flores C. A., Rauw G., 2012, A&A, 538, A22
Oskinova L. M., 2005, MNRAS, 361, 679
Oskinova L. M., Feldmeier A., Hamann W.-R., 2006, MNRAS, 372, 313

Oskinova L. M., Gayley K. G., Hamann W.-R., Huenemoerder D. P., Ignace R., Pollock A. M. T., 2012, ApJ, 747, L25
Owocki S. P., Cohen D. H., 1999, ApJ, 520, 833 (OC99)
Owocki S. P., Cohen D. H., 2001, ApJ, 559, 1108 (OC01)
Owocki S. P., Cohen D. H., 2006, ApJ, 648, 565
Owocki S. P., Puls J., 1999, ApJ, 510, 355
Owocki S. P., Castor J. I., Rybicki G. B., 1988, ApJ, 335, 914
Owocki S., Sundqvist J., Cohen D., Gayley K., 2012, in Drissen L., Robert C., St-Louis N., Moffat A., eds., ASP Conference Series, Vol. 465, Four Decades of Research on Massive Stars. Astron. Soc. Pac., San Francisco, p. 111
Parkin E. R., Pittard J. M., 2010, MNRAS, 406, 2373
Puls J., Springmann U., Lennon M., 2000, A&AS, 141, 23
Runacres M. C., Owocki S. P., 2002, A&A, 381, 1015
Sana H., Rauw G., Nazé Y., Gosset E., Vreux J., 2006, MNRAS, 372, 661
Schure K. M., Kosenko D., Kaastra J. S., Keppens R., Vink J., 2009, A&A, 508, 751
Smith R. K., Brickhouse N. S., Liedahl D. A., Raymond J. C., 2001, ApJ, 556, L91
Smith N., Conti P. S., 2008, ApJ, 679, 1467
Stevens I. R., Blondin J. M., Pollock A. M. T., 1992, ApJ, 386, 265
Sundqvist J. O., Owocki S. P., 2012, MNRAS, p. 144
Sundqvist J. O., Owocki S. P., Cohen D. H., Leutenegger M. A., Townsend R. H. D., 2012, MNRAS, 420, 1553
Vink J. S., de Koter A., Lamers H. J. G. L. M., 2000, A&A, 362, 295
Vishniac E. T., 1994, ApJ, 428, 186
Wade G. A., 2012, in Drissen L., Robert C., St-Louis N., Moffat A., eds., ASP Conference Series, Vol. 465, Four Decades of Research on Massive Stars, Astron. Soc. Pac., San Francisco, p. 33
Walder R., Folini D., 1998, A&A, 330, L21
Wojdowski P. S., Schulz N. S., 2005, ApJ, 627, 953
Zhekov S. A., Palla F., 2007, MNRAS, 382, 1124

This paper has been typeset from a TEX/LATEX file prepared by the author.